Accepted Manuscript

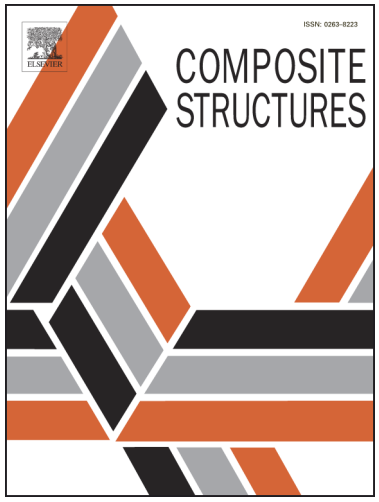

Thermal Effect and Active Control on Bistable Behaviour of Anti-symmetric Composite Shells with Temperature-dependent Properties

Zheng Zhang, Gangfei Ye, Huaping Wu, Helong Wu, Dandi Chen, Guozhong Chai

PII: S0263-8223(15)00036-7
DOI: http://dx.doi.org/10.1016/j.compstruct.2015.01.024
Reference: COST 6154

To appear in: *Composite Structures*

Please cite this article as: Zhang, Z., Ye, G., Wu, H., Wu, H., Chen, D., Chai, G., Thermal Effect and Active Control on Bistable Behaviour of Anti-symmetric Composite Shells with Temperature-dependent Properties, *Composite Structures* (2015), doi: http://dx.doi.org/10.1016/j.compstruct.2015.01.024

Thermal Effect and Active Control on Bistable Behaviour of Anti-symmetric Composite Shells with Temperature-dependent Properties

Zheng Zhang[a,*], Gangfei Ye[a], Huaping Wu[a], Helong Wu[b], Dandi Chen[a], Guozhong Chai[a]

[a]Key Laboratory of E&M (Zhejiang University of Technology), Ministry of Education & Zhejiang Province, Hangzhou 310014, P.R. China

[b]School of Civil Engineering, The University of Queensland, St Lucia, QLD 4072, Australia

*Corresponding author. E-mail address: zzhangme@zjut.edu.cn (Zheng Zhang), Telephone: 86-571-88320244.

Abstract: Anti-symmetric cylindrical shells with two stable configurations have been proved to offer novel morphing structures in advanced engineering fields. The bistable behaviour of anti-symmetric composite shells under thermomechanical loading is analyzed herein theoretically combined with a finite element modeling. The properties of the composite material in current study are considered to be functions of temperature. The shell is subjected to two different thermal load, i.e. the uniform temperature field and through-thickness thermal gradient. The influence of this two temperature field on the shell's stable shapes was predicted analytically, which thereafter is determined by finite element results. This provides a feasible approach of controlling the deformation of the bistable shell through adjusting the applied temperature field. For this purpose, a superposition of uniform temperature field and through-thickness thermal gradient is imposed and its influence on the bistable shapes of bistable shells is therefore investigated, which is of great importance to the design and application of morphing structures manufactured from bistable composite shells.

Keywords: bistable composite structure; anti-symmetric cylindrical shell; uniform temperature field; through-thickness thermal gradient; deformation control.

Nomenclature

E_1	Longitudinal modulus
E_2	Transverse modulus
G_{12}	In-plane shear modulus
k_x	Curvature in the *x* direction
k_y	Curvature in the *y* direction
k_{xy}	Twisting curvature in *x*-*y* plane in natural coordinates
k_{x1} k_{y1} k_{xy1}	Curvatures in shell's first stable state
k_{x2} k_{y2} k_{xy2}	Curvatures in shell's second stable state
k_{y1}^a k_{xy1}^a k_{x2}^a k_{xy2}^a	Analytical results of curvature
k_{y1}^f k_{xy1}^f k_{x2}^f k_{xy2}^f	Simulation results of curvature
L	Longitudinal length for the shell's initial shape
n	Number of layers
Q_{ij}^k	Stiffness coefficients for the *k*th lamina
R	Mid-plane transverse radius of the shell's first state
t	Thickness of a single layer
T	Temperature
T_0	Stress-free temperature (i.e. reference temperature)
ΔT	Change in temperature
T_z	Through-thickness thermal gradient

Vectors and matrices

$\boldsymbol{A}$	Extensional stiffness matrix
A_{ij}	*ij* element of the extensional stiffness matrix
$\boldsymbol{B}$	Coupling stiffness matrix
B_{ij}	*ij* element of the coupling stiffness matrix

$\boldsymbol{D}$	Bending stiffness matrix
D_{ij}	*ij* element of the bending stiffness matrix
Q_{ij}^{k}	*ij* element of the transformed lamina material stiffness
$\boldsymbol{N}$	External force vector
$\boldsymbol{M}$	External moment vector
$\boldsymbol{N}^{M}$	Mechanical force vector
$\boldsymbol{M}^{M}$	Mechanical moment vector
$\boldsymbol{N}^{T}$	Thermal force vector
$\boldsymbol{M}^{T}$	Thermal moment vector
$\boldsymbol{\varepsilon}$	Mid-surface strains vector
$\boldsymbol{k}$	Mid-surface curvatures vector
$\boldsymbol{\varepsilon}^{M}$	Mechanical mid-surface strains vector
$\boldsymbol{k}^{M}$	Mechanical mid-surface curvatures vector
$\boldsymbol{\varepsilon}^{T}$	Thermal mid-surface strains vector
$\boldsymbol{k}^{T}$	Thermal mid-surface curvatures vector

Greek letters

α	Ply angle of plies
α_{11}	Longitudinal thermal expansion coefficient
α_{22}	Transverse thermal expansion coefficient
α_{x}^{k}	Thermal expansion coefficient in *x*-axes in natural coordinates
α_{y}^{k}	Thermal expansion coefficient in *y*-axes in natural coordinates
α_{xy}^{k}	Thermal expansion coefficient in *x*-*y* plane in natural coordinates
γ	Angle of embrace of the shell's first state
ν	Poisson ratio

1. Introduction

Bistable composite structures have been proposed to generate novel morphing and deployable structures within a range of advanced engineering areas [1-4] for their favorable load-carrying capability, deformability and light-weight performances [5]. In particular, bistable structures are able to maintain either of two stable configurations without a continuous power supply [6-8]. Bistable composite structures, including cross-ply $[0_n/90_n]^T$ composite laminate and anti-symmetric cylindrical shell, can deform from one stable shape to another under an external stimulation induced by mechanical forces, piezoelectric patches, temperature field or SMAs (shape memory alloys) [9-12]. As the laminate structure is cured at high temperature, usually 120°C to 180°C [13, 14], leading to strains arise in the laminate and its multistability. Bistable behaviour of the plate structures is subjected to mechanical, thermal or thermomechanical loadings. As both of the structures and material of the laminate are affected by the temperature variation, the stresses and deformations induced by the temperature play the significant role in the design of the bistable composite structures.

For decades of years, the cured curvature of bistable laminates have been predicted with good precision by using analytical approaches [15-19]. The bistable behaviour of cross-ply laminated plates was firstly found using Rayleigh–Ritz method by Hyer [20]. The anti-symmetric composite cylindrical shell with two stable shapes was discovered and exploited by Daton Lovett [21] and then firstly presented by Iqbal et al. [22, 23]. Guest and Pellegrino [24] developed a simple two-parameter model which made the calculation of coiled-up radius of anti-symmetric shell easier. Zhang et al. [25, 26] presented a new experimental method by mechanical load to achieve the snapping process of the anti-symmetric shell. The required loads and shell deformation of the shell transforming between two stable configurations were given experimentally. According to the application situation of the bistable composite structures, the environmental influence on bistable behaviour and the sensitivity of material properties of the unsymmetric laminates to environmental conditions (i.e. temperature) was also considered by some researchers. Etches [27] examined the

effects of moisture absorption on the mechanical properties of thermal induced multistability laminates focusing on geometry and snap-through loadings. Most researchers focused on the temperature influence on the curing process of unsymmetric laminates. Moore et al. [28] examined the stability and thermal response of the unsymmetric laminates using a combined finite element and experiment method, and the second stable shapes were also captured at different temperatures. The resin layers and the layup thickness effects on the relationships between the temperature and curvature were also investigated simultaneously. Eckstein et al. [29] predicted the shapes of multi-stable laminated plates subjected to thermal loads by analytical method, with considering the thermal gradients and temperature-dependent material properties. Moreover, the curvatures of laminated plates subjected to thermal loads are captured by experimental method with dial-gauge rig, which shows good agreement to analytical results [30]. Brampton et al. [31] demonstrated that bistable laminates are most sensitive to uncertainties in the material properties, ply thickness and cure temperature change. It was shown that the material properties of laminates are highly sensitive to temperature and moisture absorption changes. The actuation of bistable laminates by conductive polymer nanocomposites for use in thermal-mechanical aerosurface de-icing is studied by Brampton et al. [32]. The laminate is heated from one surface to disturb the skin to initiate debond of ice-skin interface, which leads to the thermal gradient through the laminate thickness. Besides, influence of a thermo-oxidative environment (150°C under atmospheric air) on the deformation behaviour of [0/90] unsymmetric laminates is also studied by Gigliotti et al. [33, 34]. The curing process and bistable behaviours of cross-ply laminates have been studied extensively by various researchers. To the best of authors' knowledge, no previous work has been done on the thermomechanical analysis of bistable behaviour of anti-symmetric composite shells.

Thus, the purpose of this paper is to study the thermal effect on the bistable behaviour and deformation process of the anti-symmetric cylindrical shell, which is caused by the temperature influence, including the uniform temperature field and through-thickness thermal gradient. Both influences of uniform temperature field and

through-thickness thermal gradient on the curvatures of the shell are achieved by comprehensive theoretical and numerical results. Besides, combine effect of uniform temperature field and through-thickness thermal gradient variation is also studied to obtain the deformation and curvature regulation of the shell's bistable behaviour. The results of the thermal influence on the bistable behaviour of anti-symmetric bistable composite shells are helpful for the application of bistable structures in aerospace industry and so on.

2. Theoretical and numerical methodology

The study of thermal effect on the bistable behaviour of anti-symmetric cylindrical shells is based on a combined theoretical-numerical methodology. As the material properties of the shell are affected by the temperature, the anti-symmetric composite shells investigated in this paper were made from carbon/PMR-15 with temperature-dependent material [29, 35]. According to the experimental data and then through linear fitting or second-order least-square fitting, material properties are presented as followed:

$$E_1 = (-0.0525 \times T + 139.67)\text{GPa}$$

$$E_2 = (-0.0108 \times T + 9.1389)\text{GPa}$$

$$G_{12} = (5 \times 10^{-5} \times T^2 - 0.0335 \times T + 7.1771)\text{GPa}$$

$$\nu = 0.45$$

$$\alpha_{11} = (-4 \times 10^{-6} \times T^2 + 0.0022 \times T - 0.2461) \times 10^{-6} / ^\circ\text{C}$$

$$\alpha_{22} = (-0.0002 \times T^2 + 0.0229 \times T + 28.341) \times 10^{-6} / ^\circ\text{C}$$

where T is the environmental temperature in degree centigrade, E_1, E_2 and G_{12} are the longitudinal, transverse and shear modulus respectively, Poisson ratio ν for simplicity is chosen as 0.45 [35], and α_{11}, α_{22} are the longitudinal and transverse thermal expansions, respectively.

Fig. 1 depicts geometrical sizes of the anti-symmetric cylindrical shell, where R denotes the mid-plane transverse radius of the first state, γ is the angle of embrace, L

defines the longitudinal length, α is the ply angle of plies, n indicates the number of plies.

2.1 Theoretical analysis

The linear-elastic behaviour of a laminated plate is characterized by its ***ABD*** matrix which correlates the mid-surface strains and curvatures to the corresponding stress resultants in the shell. As the shell is influenced by the temperature field, the ***ABD*** matrix of a composite shell with anti-symmetric layup is including two parts: mechanical load and thermal load, as given below:

$$\begin{Bmatrix} \boldsymbol{N} \\ \boldsymbol{M} \end{Bmatrix} = \begin{Bmatrix} \boldsymbol{N}^M + \boldsymbol{N}^T \\ \boldsymbol{M}^M + \boldsymbol{M}^T \end{Bmatrix} = \begin{bmatrix} \boldsymbol{A} & \boldsymbol{B} \\ \boldsymbol{B} & \boldsymbol{D} \end{bmatrix} \begin{Bmatrix} \boldsymbol{\varepsilon} \\ \boldsymbol{k} \end{Bmatrix} = \begin{bmatrix} \boldsymbol{A} & \boldsymbol{B} \\ \boldsymbol{B} & \boldsymbol{D} \end{bmatrix} \begin{Bmatrix} \boldsymbol{\varepsilon}^M \\ \boldsymbol{k}^M \end{Bmatrix} + \begin{Bmatrix} \boldsymbol{\varepsilon}^T \\ \boldsymbol{k}^T \end{Bmatrix} \tag{1}$$

where $\boldsymbol{N}$, $\boldsymbol{M}$ are the external force and moment, $\boldsymbol{\varepsilon}$ and $\boldsymbol{k}$ are the mid-surface strains and curvatures, and the superscript M and T represent mechanical and thermal contents respectively, $\boldsymbol{A}$ represents the extensional stiffness matrix, $\boldsymbol{B}$ is the coupling stiffness matrix and $\boldsymbol{D}$ denotes the bending stiffness matrix.

Thermal force and moment $\boldsymbol{N}^T$ and $\boldsymbol{M}^T$ can be given by

$$\begin{Bmatrix} N_x^T \\ N_y^T \\ N_{xy}^T \end{Bmatrix} = \sum_{k=1}^{N} \int_{z_{k-1}}^{z_k} \begin{bmatrix} Q_{11}^k & Q_{12}^k & Q_{16}^k \\ Q_{12}^k & Q_{22}^k & Q_{26}^k \\ Q_{16}^k & Q_{26}^k & Q_{66}^k \end{bmatrix} \begin{Bmatrix} \alpha_x^k \\ \alpha_y^k \\ \alpha_{xy}^k \end{Bmatrix} \Delta T dz \tag{2}$$

$$\begin{Bmatrix} M_x^T \\ M_y^T \\ M_{xy}^T \end{Bmatrix} = \sum_{k=1}^{N} \int_{z_{k-1}}^{z_k} \begin{bmatrix} Q_{11}^k & Q_{12}^k & Q_{16}^k \\ Q_{12}^k & Q_{22}^k & Q_{26}^k \\ Q_{16}^k & Q_{26}^k & Q_{66}^k \end{bmatrix} \begin{Bmatrix} \alpha_x^k \\ \alpha_y^k \\ \alpha_{xy}^k \end{Bmatrix} \Delta T z dz \tag{3}$$

where Q_{ij}^k are transformed lamina material stiffness, ΔT is the change in temperature, α_x^k, α_y^k and α_{xy}^k are thermal expansions in x and y-axes and x-y plane in natural coordinates respectively, and

$$\begin{Bmatrix} \alpha_x^k \\ \alpha_y^k \\ \alpha_{xy}^k \end{Bmatrix} = \begin{bmatrix} \cos^2\alpha & \sin^2\alpha & -\sin\alpha\cos\alpha \\ \sin^2\alpha & \cos^2\alpha & \sin\alpha\cos\alpha \\ 2\sin\alpha\cos\alpha & -2\sin\alpha\cos\alpha & \cos^2\alpha - \sin^2\alpha \end{bmatrix} \begin{Bmatrix} \alpha_{11} \\ \alpha_{22} \\ 0 \end{Bmatrix} \tag{4}$$

Then the thermal strain and curvature are obtained by

$$\begin{Bmatrix} \boldsymbol{\varepsilon}^T \\ \boldsymbol{k}^T \end{Bmatrix} = \begin{bmatrix} \boldsymbol{A} & \boldsymbol{B} \\ \boldsymbol{B} & \boldsymbol{D} \end{bmatrix}^{-1} \begin{Bmatrix} \boldsymbol{N}^T \\ \boldsymbol{M}^T \end{Bmatrix} \tag{5}$$

The ***ABD*** matrix for a composite shell with antisymmetric lay-up is given as:

$$\begin{Bmatrix} N_x \\ N_y \\ N_{xy} \\ M_x \\ M_y \\ M_{xy} \end{Bmatrix} = \begin{bmatrix} A_{11} & A_{12} & 0 & 0 & 0 & B_{16} \\ A_{12} & A_{22} & 0 & 0 & 0 & B_{26} \\ 0 & 0 & A_{66} & B_{16} & B_{26} & 0 \\ 0 & 0 & B_{16} & D_{11} & D_{12} & 0 \\ 0 & 0 & B_{26} & D_{12} & D_{22} & 0 \\ B_{16} & B_{26} & 0 & 0 & 0 & D_{66} \end{bmatrix} \begin{bmatrix} \varepsilon_x \\ \varepsilon_y \\ \gamma_{xy} \\ k_x \\ k_y \\ k_{xy} \end{bmatrix} \tag{6}$$

The coiled-up radii can be achieved by reaching the minimum value of the total strain energy, which includes both the bending strain energy and the stretching strain energy. The bending strain energy and stretching strain energy per unit area in the mid-surface of a laminated plate are as followed respectively [36]

$$\begin{aligned} u_b = \frac{1}{2}(M_x k_x + M_y k_y + M_{xy} k_{xy}) = \frac{1}{2}(A_{11}\varepsilon_x{}^2 + A_{12}\varepsilon_x\varepsilon_y + B_{16}\varepsilon_x k_{xy} \\ + A_{12}\varepsilon_x\varepsilon_y + A_{22}\varepsilon_y{}^2 + B_{26}\varepsilon_y k_{xy} + A_{66}\gamma_{xy}{}^2 + B_{16}\gamma_{xy}k_x + B_{26}\gamma_{xy}k_y) \end{aligned} \tag{7}$$

$$\begin{aligned} u_s = \frac{1}{2}(N_x\varepsilon_x + N_y\varepsilon_y + N_{xy}\gamma_{xy}) = \frac{1}{2}(B_{16}\gamma_{xy}k_x + D_{11}k_x{}^2 + D_{12}k_x k_y \\ + B_{26}\gamma_{xy}k_y + D_{12}k_x k_y + D_{22}k_y{}^2 + B_{16}\varepsilon_x k_{xy} + B_{26}\varepsilon_y k_{xy} + D_{66}k_{xy}{}^2) \end{aligned} \tag{8}$$

The total strain energy per unit area in the mid-surface of a laminated plate is

$$\begin{aligned} u = u_s + u_b = \frac{1}{2}(A_{11}\varepsilon_x{}^2 + 2A_{12}\varepsilon_x\varepsilon_y + 2B_{16}\varepsilon_x k_{xy} + 2B_{26}\varepsilon_y k_{xy} + A_{22}\varepsilon_y{}^2 + A_{66}\gamma_{xy}{}^2 \\ + 2B_{16}\gamma_{xy}k_x + 2B_{26}\gamma_{xy}k_y + D_{11}k_x{}^2 + 2D_{12}k_x k_y + D_{22}k_y{}^2 + D_{66}k_{xy}{}^2) \end{aligned} \tag{9}$$

γ_{xy} can be achieved from matrix conversion $\boldsymbol{\varepsilon^0} = \boldsymbol{A}^{-1}(\boldsymbol{N} - \boldsymbol{B}\boldsymbol{k}) = \boldsymbol{A}^{-1}\boldsymbol{N} - \boldsymbol{A}^{-1}\boldsymbol{B}\boldsymbol{k}$

$$\gamma_{xy} = C_{61}k_x + C_{62}k_y \tag{10}$$

where C_{61} and C_{62} can be obtained from the matrix $\boldsymbol{C} = \text{-}\boldsymbol{A}^{-1}\boldsymbol{B}$.

Substituting Eq. (10) into Eq. (9) gives

$$\begin{aligned} u = \frac{1}{2}[A_{11}\varepsilon_x{}^2 + 2A_{12}\varepsilon_x\varepsilon_y + 2B_{16}\varepsilon_x k_{xy} + 2B_{26}\varepsilon_y k_{xy} + A_{22}\varepsilon_y{}^2 \\ + (D_{11} + B_{16}C_{61})k_x{}^2 + (2D_{12} + B_{16}C_{62} + B_{26}C_{61})k_x k_y + D_{22}k_y{}^2 + D_{66}k_{xy}{}^2] \end{aligned} \tag{11}$$

The curvatures in second stable state can be defined as k_{x2}, k_{y2} and k_{xy2}, and thermal strains and curvatures are represented by ε_x^T, ε_y^T, γ_{xy}^T, k_x^T, k_y^T and k_{xy}^T. Substituting $\varepsilon_x = \varepsilon_x^0 + \varepsilon_x^T$, $\varepsilon_y = \varepsilon_y^0 + \varepsilon_y^T$, $\gamma_{xy} = C_{61}k_x + C_{62}k_y + \gamma_{xy}^T$, $k_x = k_{x2} - k_x^T$, $k_y = k_{y2} - 1/R - k_y^T$, $k_{xy} = k_{xy2} - k_{xy}^T$ into Eq. (11)

$$\begin{aligned} u = \frac{1}{2}[&A_{11}(\varepsilon_x^0)^2 + 2A_{11}\varepsilon_x^0\varepsilon_x^T + A_{11}(\varepsilon_x^T)^2 + 2A_{12}(\varepsilon_x^0 + \varepsilon_x^T)(\varepsilon_y^0 + \varepsilon_y^T) \\ &+ 2B_{16}(\varepsilon_x^0 + \varepsilon_x^T)(k_{xy2} - k_{xy}^T) + 2B_{26}(\varepsilon_y^0 + \varepsilon_y^T)(k_{xy2} - k_{xy}^T) + A_{22}(\varepsilon_y^0 + \varepsilon_y^T)^2 \\ &+ (D_{11} + B_{16}C_{61})k_x^2 + (2D_{12} + B_{16}C_{62} + B_{26}C_{61})(k_{x2} - k_x^T)(k_{y2} - 1/R - k_y^T) \\ &+ D_{22}(k_{y2} - 1/R - k_y^T)^2 + D_{66}(k_{xy2} - k_{xy}^T)^2 + A_{66}(\gamma_{xy}^T)^2] \end{aligned} \tag{12}$$

where $\varepsilon_x^0 = [\dfrac{2\sin(\gamma R k_{y2}/2)}{\gamma R k_{y2}^2} - \dfrac{\cos\theta}{k_{y2}}]k_{x2}$, $\varepsilon_y^0 \approx 0$ [23].

Then the total strain energy is obtained by integral method of Eq. (12)

$$\begin{aligned} U = &\frac{1}{2}LA_{11}[\frac{\gamma R k_{x2}^2}{2k_{y2}^2} + \frac{\sin(\gamma R k_{y2})k_{x2}^2}{2k_{y2}^3} - \frac{4\sin^2(\gamma R k_{y2}/2)k_{x2}^2}{\gamma R k_{y2}^4}] \\ &+ \frac{1}{2}\gamma LR[A_{11}(\varepsilon_x^T)^2 + 2A_{12}\varepsilon_x^T\varepsilon_y^T + 2B_{16}\varepsilon_x^T(k_{xy2} - k_{xy}^T) + 2B_{26}\varepsilon_y^T(k_{xy2} - k_{xy}^T) + A_{22}(\varepsilon_y^T)^2 \\ &+ (D_{11} + B_{16}C_{61})k_{x2}^2 + (2D_{12} + B_{16}C_{62} + B_{26}C_{61})(k_{x2} - k_x^T)(k_{y2} - 1/R - k_y^T) \\ &+ D_{22}(k_{y2} - 1/R - k_y^T)^2 + D_{66}(k_{xy2} - k_{xy}^T)^2 + + A_{66}(\gamma_{xy}^T)^2] \end{aligned} \tag{13}$$

Bistable solutions for an anti-symmetric shell are reached at the minimum value of the total strain energy. Considering the transverse curvature approximates 0 in the second stable state $k_{y2} \approx 0$, the principal curvature k_{x2} and twisting curvature k_{xy2} in the second stable state can be shown as

$$\frac{dU}{dk_{x2}} = 0 \Rightarrow k_{x2} = \frac{(2D_{12} + B_{16}C_{62} + B_{26}C_{61})}{2R(D_{11} + B_{16}C_{61})} + k_x^T \tag{14}$$

$$\frac{dU}{dk_{xy2}} = 0 \Rightarrow k_{xy2} = -\frac{B_{16}\varepsilon_x^T + B_{26}\varepsilon_y^T}{D_{66}} + k_{xy}^T \tag{15}$$

where ε_x^T, ε_y^T, k_x^T and k_{xy}^T are achieved from Eq. (5).

2.2 Numerical simulation

A finite element analysis (FEA) of the thermal influence on the bistable

behaviour of the shell using ABAQUS is conducted. A simplified model of the anti-symmetric shell is built as shown in Fig. 2. The geometric parameters of first stable configuration are: L=100mm, R=25mm, γ=180°, thickness of lamina t=0.125mm and the layup is [45°/-45°/45°/-45°]. As the material properties of the shell are affected by temperature obviously, the input material properties are temperature-dependent. The shell changes between two stable states by applying moment on the straight shell edges, with its center's "*Displacement/Rotation*" boundary conditions constrained. S4R reduced integration shell element is chosen here for better convergence.

Three steps are included in the present FE analysis: (1) The temperature is applied on the shell by option *predefined field*, leading to the temperature of the shell reaching to the needed level. (2) *Shell edge moments* are loaded on the straight edges of the shell in order to make the shell snap from first state to the second state. (3) Remove the *Shell edge moments* and relax the shell to the second stable state. The snapping process is shown in Fig. 3.

3. Results and discussion

As the bistable shell has the potential in the application in the morphing wing of aricraft, it can be influenced by both of uniform temperature field and through-thickness thermal gradient. Considering the thermal influence is made up of three parts, a linear through-thickness temperature variation given by

$$T = T_0 + \Delta T + T_z z \tag{16}$$

where T_0 is the stress-free temperature (i. e. reference temperature 20°C), ΔT is the variation of uniform temperature field, and T_z is the through-thickness thermal gradient.

3.1 Uniform temperature field (UTF)

Assuming T_0 is 20°C, T_z is 0°C and only variation of uniform temperature field ΔT is considered in this case. According to working situation and material's

limit of the anti-symmetric shell, the range of temperature T is chosen from -50°C to 350°C, which means ΔT varies from -70°C to 330°C. The theoretical prediction of ΔT on the principal curvature in the second stable state k_{x2} is shown in Fig. 4. k_{x2} is equal to 27.01 m^{-1} when environmental temperature remains unchanged, as shown by point **A** in Fig. 4. The k_{x2} has an approximately linear relationship with ΔT increasing from -70°C before decreasing from 200°C. As ΔT increases, the radius of the anti-symmetric shell's second state increases.

As before mentioned in theoretical analysis, $k_{xy} \neq 0$ from theoretical results, the anti-symmetric shell twists as a result of the variation of uniform temperature field ΔT. The effects of temperature variation on the twisting curvatures of anti-symmetric composite shells are shown in Fig. 5, where k_{xy1} and k_{xy2} are the twisting curvatures of initial and second stable shapes respectively. It is observed that when ΔT is 0°C, namely no thermal loading is applied on the shell, both k_{xy1} and k_{xy2} are zero, which indicates that there is no twisting deformation when the shell is subjected to moments only. The overall trends of influence of ΔT on k_{xy1} and k_{xy2} are similar: k_{xy1} and k_{xy2} increase steadily until ΔT reaching 225°C from which they begin decrease gradually. It also should be noted that the twisting curvature of the second stable shape is larger than that of the initial shape for the shell.

The influence of environmental temperature (T) on bistable behaviour of an anti-symmetric composite shell is studied through theoretical analysis and numerical simulation. The theoretical and FE predicted curvatures of the shell subjected to different temperature are compared in Table 1. The analytical results of k_{x2}, denoted as k_{x2}^{a}, grow linearly with the temperature increasing and agree well with the FE predictions. Temperature similar varying trend is observed for twisting curvature k_{xy}, which means higher temperature on the shell will leads to larger torsion deformation. This can be seen clearly from Fig. 6 where the FE predicted second stable

configurations of the shell subjected different temperature fields are given for a brief comparison.

3.2 *Through-thickness thermal gradient (TTG)*

This section is to study the influence of through-thickness thermal gradient on bistable behaviour of the anti-symmetric cylindrical shell. In order to ensure that the range of the shell's temperature is -50°C to 350°C according to the limit of the shell's material properties, the midplane temperature is chosen as 150°C, and the through-thickness thermal gradient T_z is assumed to range from -800°C mm^{-1} to 800°C mm^{-1} along the thickness direction. The positive and negative signs of T_z are defined in Fig. 7, where temperature increasing from bottom to top surface is defined as positive (Fig. 7a). On the contrary, the thermal gradient is negative (Fig. 7b). The impacts of T_z on the bistable shapes of the shell are shown in Fig. 8 from which we can see that both k_{xy1} and k_{xy2} are negative and vary symmetrically about T_z=0°C. This means k_{xy} is only dependent of the magnitude of T_z. When T_z increases from 0°C mm^{-1} to ±800°C mm^{-1}, k_{xy} decreases from 0 mm^{-1} to less than -1.8 mm^{-1}, which means that the influence of T_z on k_{xy} is slight. In Fig. 8a, it can be observed that the initial principal curvature k_{y1} gradually grows with the increment of T_z, while the principal curvature in the second stable state k_{x2} increases until T_z=500°C mm^{-1}, followed by a trend of decreasing.

With a range of -500°C mm^{-1} to 500°C mm^{-1} with an interval of 100 for T_z, the analytical and FE predicted curvatures versus T_z curves for the shell are plotted in Fig. 9. According to theoretical analysis, T_z has a greater effect on the values of k_y and k_x than that of k_{xy}, which agree well with the FE predictions. As can be seen from Fig. 9, k_{y1} and k_{x2} increase with an approximate slope with the T_z rising at

the given range. It is observed that the FE results have a good agreement with analytical predictions.

3.3 Combination of UTF and TTG

This section is to investigate the bistable behaviour of the cylindrical composite shell under an overlapped temperature field of *UTF* and *TTG*. The variation of uniform temperature field ΔT changes from 30°C to 105°C, and the magnitude of through-thickness thermal gradient T_z changes from 200°C mm^{-1} to 500°C mm^{-1}. When temperature of shell's bottom surface (T_1) is assumed to keep as 0°C, the corresponding temperature of shell's mid-plane (T_2) thus varies from 50°C to 125°C and the counterpart for top surface (T_3) is from 100°C to 250°C due to the shell's thickness of 0.5 mm. For example, when the temperature of bottom surface is 0°C and T_z = 200°C mm^{-1}, the temperature distribution is shown in Fig. 10.

The direction of through-thickness thermal gradient is also considered to study the complex impact of ΔT and T_z in order to tell the importance of their influence. The analysis results are listed in Table 2. When the direction of T_z is positive, the influence of combine impact of ΔT and T_z is obviously larger than single factor's influence. As the direction of T_z has little effect on the magnitude of k_{xy}, the values of k_{xy} hardly change. But the principal curvatures k_{y1} and k_{x2} are larger when the direction of T_z is positive. However, k_{x2} and k_{xy} still increase more slowly when the direction of T_z is negative. It is because that ΔT makes k_{x2} still increase and T_z leads to the decrease of k_{x2}, but the influence of ΔT is more important than that of T_z in this condition.

4. Active control of bistable behaviour through a combined temperature field of UTF and TTG

Based on the above theoretical and FE analysis, as well as the corresponding results, it is possible to control to the bistable shapes of anti-symmetric composite shells through applying different types of temperature field.

In present FE analysis, the cylindrical shell is evenly divided into two segments, with eight subparts for each. As Fig.11 shows, these subparts are numbered from 1 to 8. The subparts with same number are centrosymmetric with respect to the centroid of the shell. Under the reference temperature (i.e. 20°C), the k_{xy} is zero since there is no twisting deformation in the shell, and the principal curvature in the second stable state k_{x2} is 24.29 m^{-1}. After applying a 150°C uniform temperature field, i.e. temperature increment ΔT =130°C, the shell will deformed into the shape of $k_{xy1} = 2.50\text{m}^{-1}$, $k_{x2} = 30.62\text{m}^{-1}$ and $k_{xy2} = 3.42\text{m}^{-1}$.

4.1 Impact of TTG magnitude

Table 3 tabulates the influence of thermal gradient T_z on the shell's geometric configuration When the value of T_z is large enough, k_{xy} caused by ΔT can still decrease. The anti-symmetric cylindrical shell twists less when $T_z = \pm 800\,°\text{C mm}^{-1}$. As can be seen in the table, both k_{y1} and k_{x2} increase slightly with the T_z changing from -800°C mm^{-1} to 800°C mm^{-1}.

4.2 Impact of different imposed area of TTG

According to the analysis above, it is reasonable to adjust the shape when T_z =-800°C mm^{-1}, which makes k_{x2} and k_{xy} decrease more closely to the result with no thermal influence. Table 4 gives the influence of local temperatures with different imposed area on the entire shell's geometric configuration. It can be observed that all curvatures listed in Table 4 decrease with the increase of temperature imposed area

under a constant T_z. The k_{x2} and k_{xy1} are approaching the results with no thermal influence.

4.3 Impact of different imposed area with different TTG direction

The influence of different through-thickness thermal gradient directions of T_z when ΔT =130°C is given in Table 5. It is novel to find out that the principal curvatures k_{y1} and k_{x2} almost keep stable when T_z is applied on different regions with positive and negative direction. The principal curvature k_{y1} keeps 39.88mm^{-1}, which is very close to the result of 40mm^{-1} without thermal influence. However, the twisting curvature k_{xy} decreases with the increase of the imposing T_z region size. It's useful to improve the shell's twist performance, which can be achieved by applying ΔT on different regions with both positive and negative directions.

Twist of the anti-symmetric shell caused by ΔT is not expected in its application, which leads to the undesirable deformation of the bistable structure. According to the results presented before, the shape of the shell can be adjusted by applying T_z when it is affected by ΔT. Comparing the results of different magnitude, applied regions and directions of T_z, the magnitude and applied region are large enough to weaken the twist of the shell. However, k_{y1} and k_{x2} are also influenced which is undesired in some conditions. It is found from the results of Table 5 that only k_{xy} is changed but k_{y1} and k_{x2} keep stable, which is satisfied to the requirement that only the twist of the shell is adjusted. Anyhow, it's useful for avoiding the thermal effect on the bistable shapes through actively applied suitable uniform temperature field and through-thickness thermal gradients.

5. Conclusion

Thermal effect and active control on the bistable behaviour of the anti-symmetric cylindrical shell is investigated through theoretical and FE analysis. According to

theoretical and FE results, both of the uniform temperature field and through-thickness thermal gradients have a significant effect on the second stable curvature k_{x2} of the anti-symmetric composite shell. The twisting curvature k_{xy} is mostly caused by the variation of uniform temperature field. Moreover, the shape of the bistable composite shell can be adjusted through imposing single or different combination of uniform temperature field and through-thickness thermal gradients. Therefore, the theoretical and numerical analysis of thermal effect on the bistable behaviour of the anti-symmetric cylindrical shell in this paper is expected to provide a prediction for the design, manufacture and application of anti-symmetric bistable composite structures.

Acknowledgement

This research was supported by the Natural Science Foundation of China (Grant No. 51205355, 11372280), the Research Fund for the Doctoral Program of Higher Education of China (Grant No. 20123317120003), the Postdoctoral Science Foundation of China (Grant No. 2013M540498).

References

[1] Hufenbach W, Gude M, Czulak A. Actor-initiated snap-through of unsymmetric composites with multiple deformation states. J Mater Process Tech, 2006; 175(1): 225-30.

[2] Schultz MR. A concept for airfoil-like active bistable twisting structures. J Intell Mater Syst Struct, 2008; 19(2): 157-69.

[3] Daynes S, Weaver PM, Potter KD. Aeroelastic Study of Bistable Composite Airfoils. J Aircraft, 2009; 46(6): 2169-74.

[4] Panesar AS, Weaver PM. Optimisation of blended bistable laminates for a morphing flap. Compos Struct, 2012; 94(10): 3092-105.

[5] Lachenal X, Daynes S, Weaver PM. Review of morphing concepts and materials for wind turbine blade applications. Wind Energy, 2013; 16(2): 283-307.

[6] Schultz MR, Hyer MW. Snap-through of unsymmetric cross-ply laminates using piezoceramic actuators. J Intell Mater Syst Struct, 2003; 14(12): 795-814.

[7] Giddings P, Bowen CR, Butler R, Kim HA. Characterisation of actuation properties of piezoelectric bi-stable carbon-fibre laminates. Compos Part A Appl Sci Manuf, 2008; 39(4): 697-703.

[8] Bowen CR, Butler R, Jervis R, Kim HA, Salo AIT. Morphing and Shape Control using Unsymmetrical Composites. J Intell Mater Syst Struct, 2006; 18(1): 89-98.

[9] Dano M-L, Hyer M. Snap-through of unsymmetric fiber-reinforced composite laminates. Int J Solids Struct, 2002; 39(1): 175-98.

[10] Dai F, Li H, Du S. A multi-stable lattice structure and its snap-through behavior among multiple states. Compos Struct, 2013; 97: 56-63.

[11] Giddings PF, Kim HA, Salo AIT, Bowen CR. Modelling of piezoelectrically actuated bistable composites. Mater Lett, 2011; 65(9): 1261-3.

[12] Dano ML, Hyer MW. SMA-induced snap-through of unsymmetric fiber-reinforced composite laminates. Int J Solids Struct, 2003; 40(22): 5949-72.

[13] Dano ML, Hyer MW. Thermally-induced deformation behavior of unsymmetric laminates. Int J Solids Struct, 1998; 35(17): 2101-20.

[14] Daynes S, Potter KD, Weaver PM. Bistable prestressed buckled laminates. Compos Sci Technol, 2008; 68(15): 3431-7.

[15] Hyer MW. The room-temperature shapes of four-layer unsymmetric cross-ply laminates. J Compos Mater, 1982; 16(4): 318-40.

[16] Jun W, Hong C. Effect of residual shear strain on the cured shape of unsymmetric cross-ply thin laminates. Compos Sci Technol, 1990; 38(1): 55-67.

[17] Pirrera A, Avitabile D, Weaver PM. Bistable plates for morphing structures: A refined analytical approach with high-order polynomials. Int J Solids Struct, 2010; 47(25): 3412-25.

[18] Zhang Z, Wu H, Wu H, He X, Bao Y, Chai G. Bistable Characteristics of Irregular Anti-symmetric Lay-up Composite Cylindrical Shells. Int J Struct Stab Dy, 2013, 13(6): 1350029.

[19] Cantera M A, Romera JM, Adarraga I, Mujika F. Modelling of [0/90] laminates

subject to thermal effects considering mechanical curvature and through-the-thickness strain. Compos Struct, 2014; 110: 77-87.

[20] Hyer MW. Calculations of the room-temperature shapes of unsymmetric laminates. J Compos Mater, 1981; 15: 296-310.

[21] Daton-Lovett A. An extendible member. Patent Cooperation Treaty Application. PCT/GB97/00839; 1996.

[22] Iqbal K, Pellegrino S. Bi-stable composite shells. In Proceedings of the 41st AIAA/ASME/ASCE/AHS/ASC Structures, Structural Dynamics, and Materials Conference and Exhibit; 2000, 3(6).

[23] Iqbal K, Pellegrino S, Daton-Lovett A. Bi-stable composite slit tubes. In: IUTAM-IASS Symposium on Deployable Structures: Theory and Applications. Springer Netherlands; 2000. p. 153-162.

[24] Guest SD, Pellegrino S. Analytical models for bistable cylindrical shells. Philos Trans R Soc Lond A 2006; 462(2067): 839-854.

[25] Zhang Z, Wu H, He X, Wu H, Bao Y, Chai G. The bistable behaviors of carbon-fiber/epoxy anti-symmetric composite shells. Compos Part B Eng, 2013; 47: 190-9.

[26] Zhang Z, Wu H, Ye G, Wu H, He X, Chai G. Systematic experimental and numerical study of bistable snap processes for anti-symmetric cylindrical shells. Compos Struct, 2014; 112: 368-77.

[27] Etches J, Potter K, Weaver P, Bond I. Environmental effects on thermally induced multistability in unsymmetric composite laminates. Compos Part A Appl Sci Manuf, 2009; 40(8): 1240-7.

[28] Moore M, Ziaei-Rad S, Salehi H. Thermal response and stability characteristics of bistable composite laminates by considering temperature dependent material properties and resin layers. Appl Compos Mater, 2013; 20(1): 87-106.

[29] Eckstein E, Pirrera A, Weaver PM. Morphing high-temperature composite plates utilizing thermal gradients. Compos Struct, 2013; 100: 363-72.

[30] Eckstein E, Pirrera A, Weaver PM. Multi-mode morphing using initially curved composite plates. Compos Struct, 2014; 109: 240-45.

[31] Brampton CJ, Betts DN, Bowen CR, Kim HA. Sensitivity of bistable laminates to uncertainties in material properties, geometry and environmental conditions. Compos Struct, 2013; 102: 276-86.

[32] Brampton C J, Bowen C R, Buschhorn S T, et al. Actuation of bistable laminates by conductive polymer nanocomposites for use in thermal-mechanical aerosurface de-icing systems. In 55th AIAA/ASMe/ASCE/AHS/SC Structures, Structural Dynamics, and Materials Conference, 2014.

[33] Gigliotti M, Grandidier JC, Lafarie-Frenot MC. The employment of 0/90 unsymmetric samples for the characterisation of the thermo-oxidation behaviour of composite materials at high temperatures. Compos Struct, 2011; 93(8): 2109-19.

[34] Gigliotti M, Pannier Y, Minervino M, Lafarie-Frenot MC, Corigliano P. The effect of a thermo-oxidative environment on the behaviour of multistable [0/90] unsymmetric composite plates. Compos Struct, 2013, 106: 863-72.

[35] Odegard G, Kumosa M. Elastic-plastic and failure properties of a unidirectional carbon/PMR-15 composite at room and elevated temperatures. Compos Sci Technol, 2000; 60(16): 2979-88.

[36] Mansfield EH. The bending and stretching of plates: Cambridge University Press; 2005.

Fig. 1 The geometrical sizes of the anti-symmetric cylindrical shell.

Fig. 2 Model of the anti-symmetric shell in FEA.

Fig. 3 Deformation process of the anti-symmetric composite shell.

Fig. 4 Theoretical prediction of the relationship between ΔT and k_{x2}.

Fig. 5 Theoretical prediction of the relationship between ΔT and k_{xy}.

Fig. 6 FE predicted second stable shapes at different temperatures: (a) 40°C and (b) 150°C.

Fig. 7 The direction of thermal gradient, the arrow indicates the direction of temperature rise.

(a) Positive direction of thermal gradient

(b) Negative direction of thermal gradient

Fig. 8 Theoretical prediction of the relationship between T_z and curvatures.

(a) Influence of T_z on initial shape of the shell.

(b) Influence of T_z on second stable shape of the shell

Fig.9 Influence of T_z on the curvatures of the shell.

(a) Relationship of T_z and the curvatures of initial shape.

(b) Relationship of T_z and the curvatures of second stable shape.

Fig. 10 Temperature distribution across shell's thickness (T_z = 200°C mm^{-1}).

Fig.11 Partition of the shell model in FE simulation.

Table 1 Influence of temperature on the curvatures of the anti-symmetric shell

Table 2 Complex impact of ΔT and T_z on the curvature of the anti-symmetric shell when T_z is applied in negative direction

Table 3 Influence of value and direction of T_z applied on all region of the shell when ΔT =130°C

Table 4 Influence of temperature field imposed of T_z when ΔT =130°C

Table 5 Influence of region with different directions of T_z when ΔT =130°C

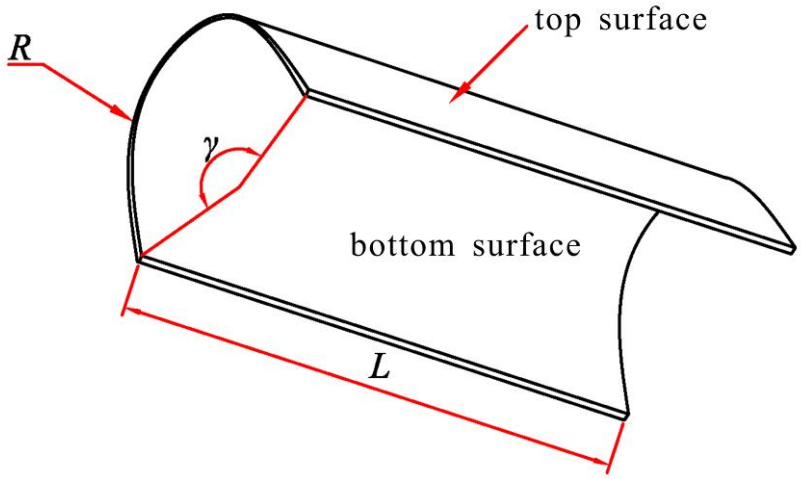

Fig. 1 The geometrical sizes of the anti-symmetric cylindrical shell.

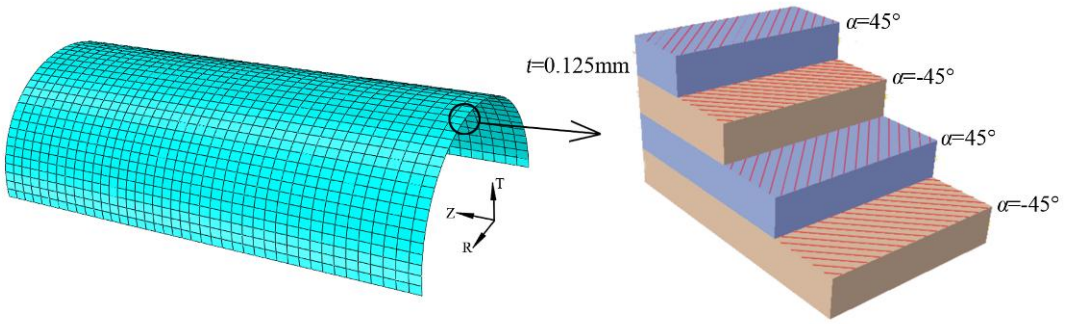

Fig. 2 Model of the anti-symmetric shell in FEA.

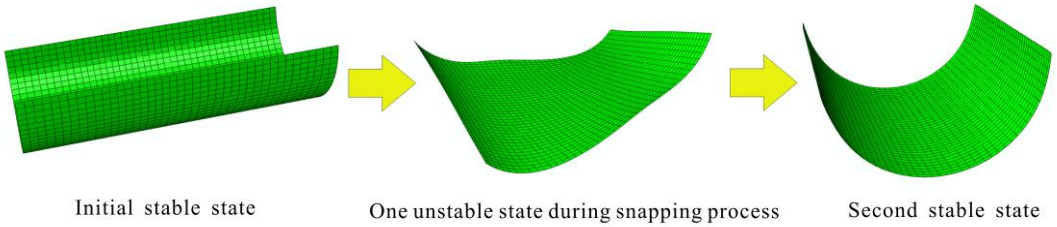

Fig. 3 Deformation process of the anti-symmetric composite shell.

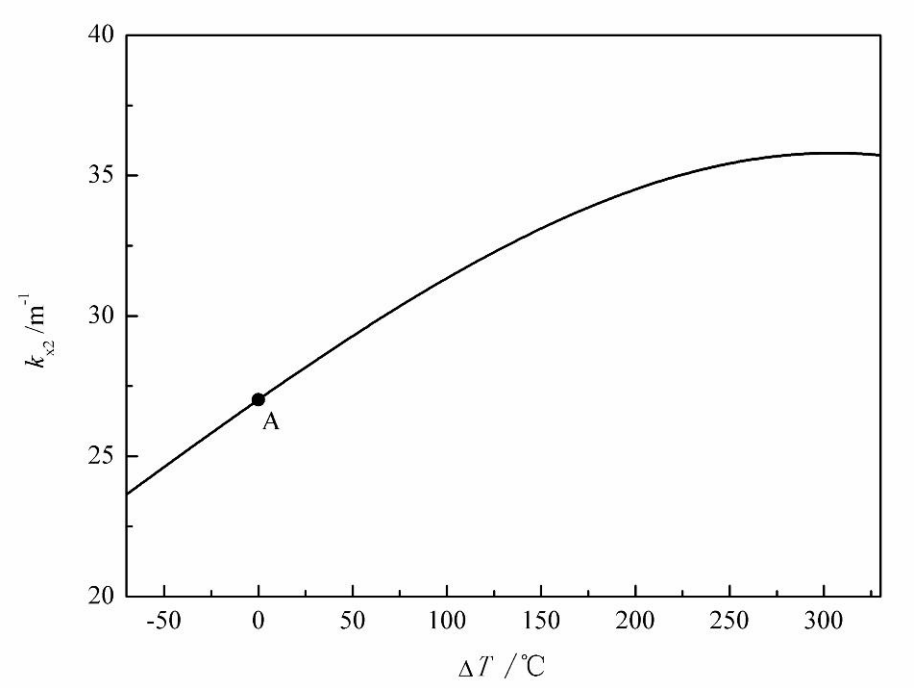

Fig. 4 Theoretical prediction of the relationship between ΔT and k_{x2}.

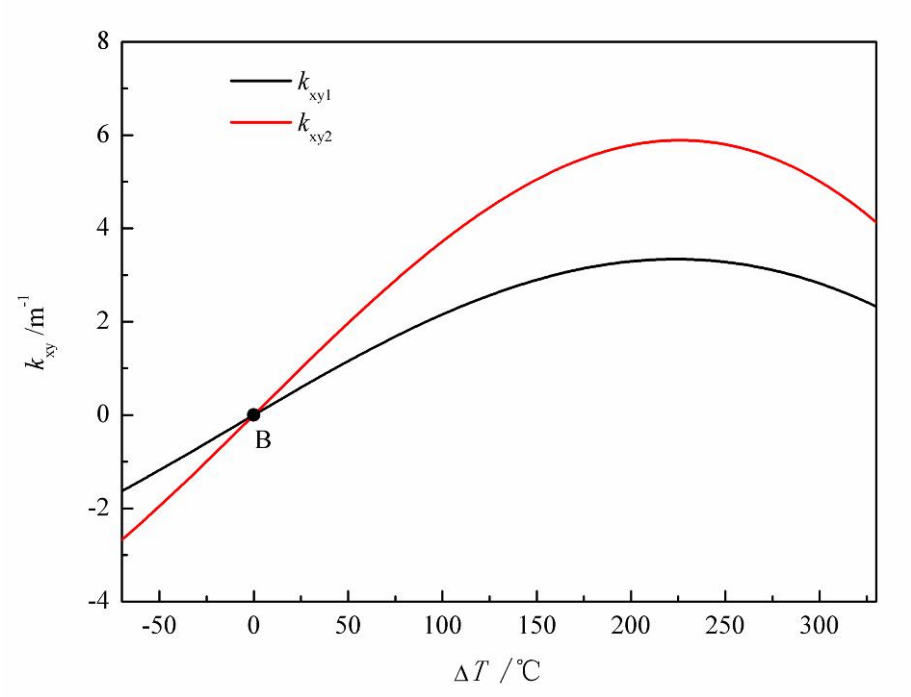

Fig. 5 Theoretical prediction of the relationship between ΔT and k_{xy}.

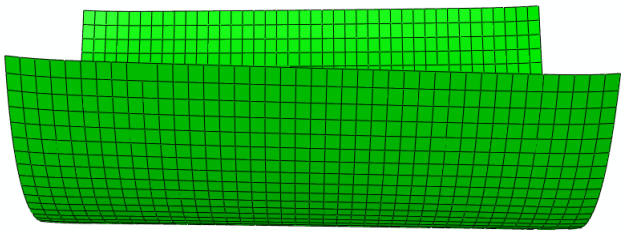

(a)

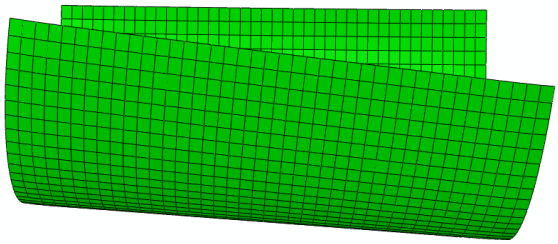

(b)

Fig. 6 FE predicted second stable shapes at different temperatures: (a) 40°C and (b) 150°C.

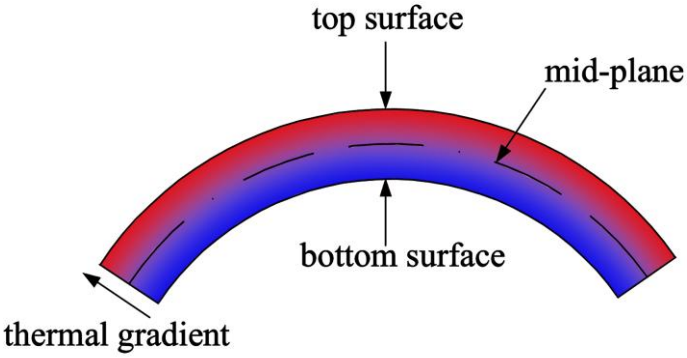

(a) Positive direction of thermal gradient

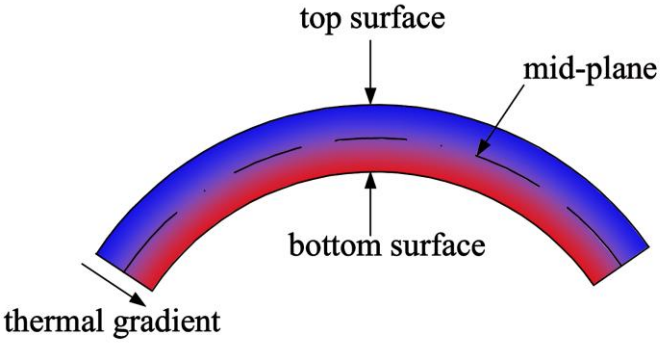

(b) Negative direction of thermal gradient

Fig. 7 The direction of thermal gradient, the arrow indicates the direction of temperature rise.

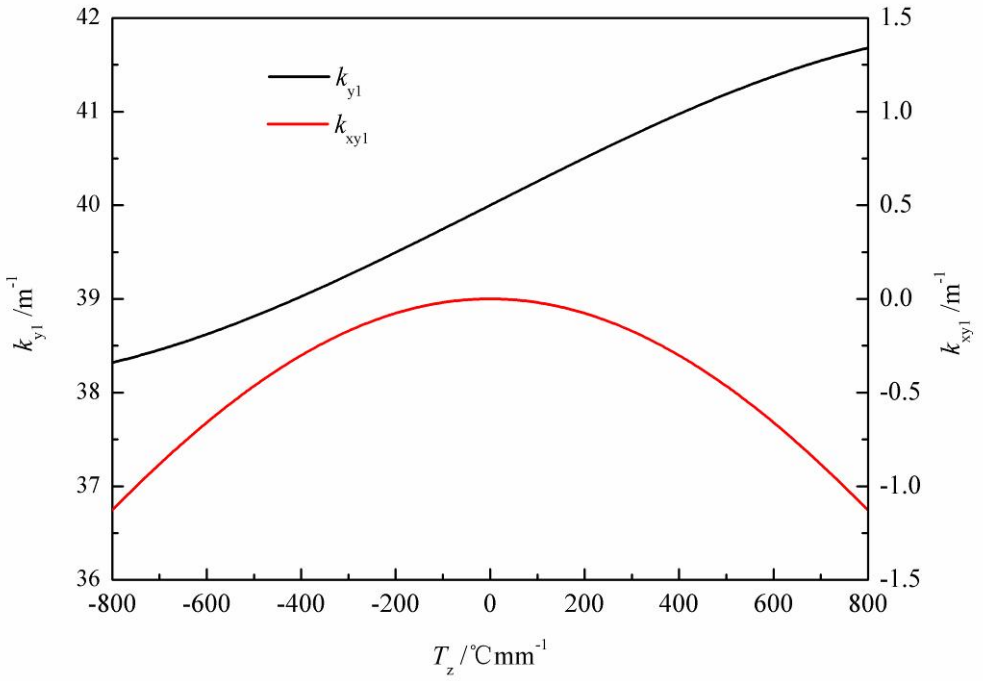

(a) Influence of T_z on initial shape of the shell

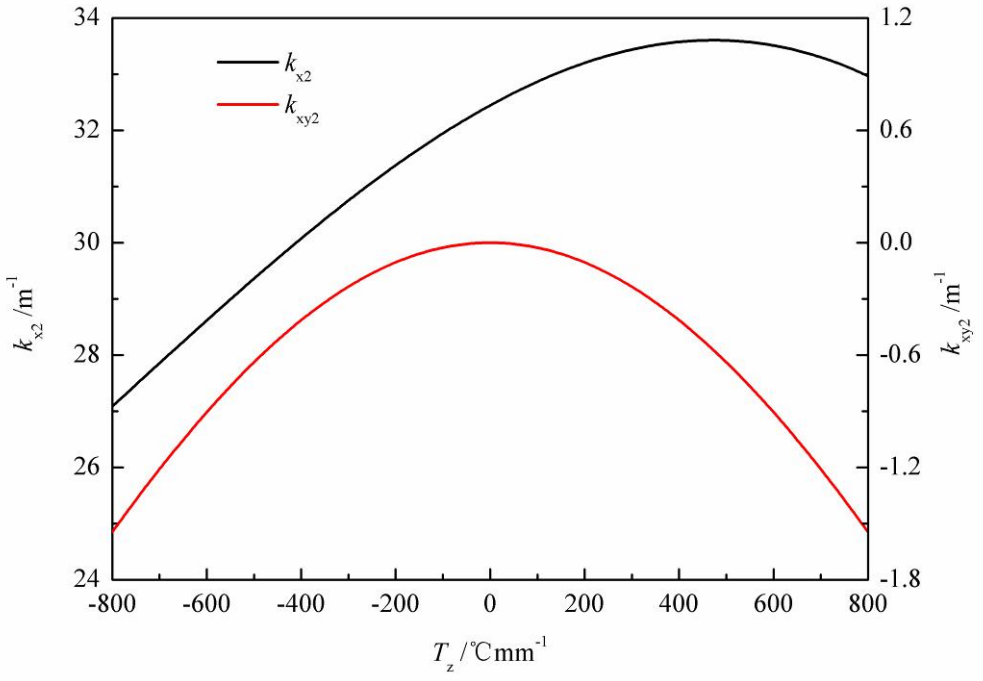

(b) Influence of T_z on second stable shape of the shell

Fig. 8 Theoretical prediction of the relationship between T_z and curvatures

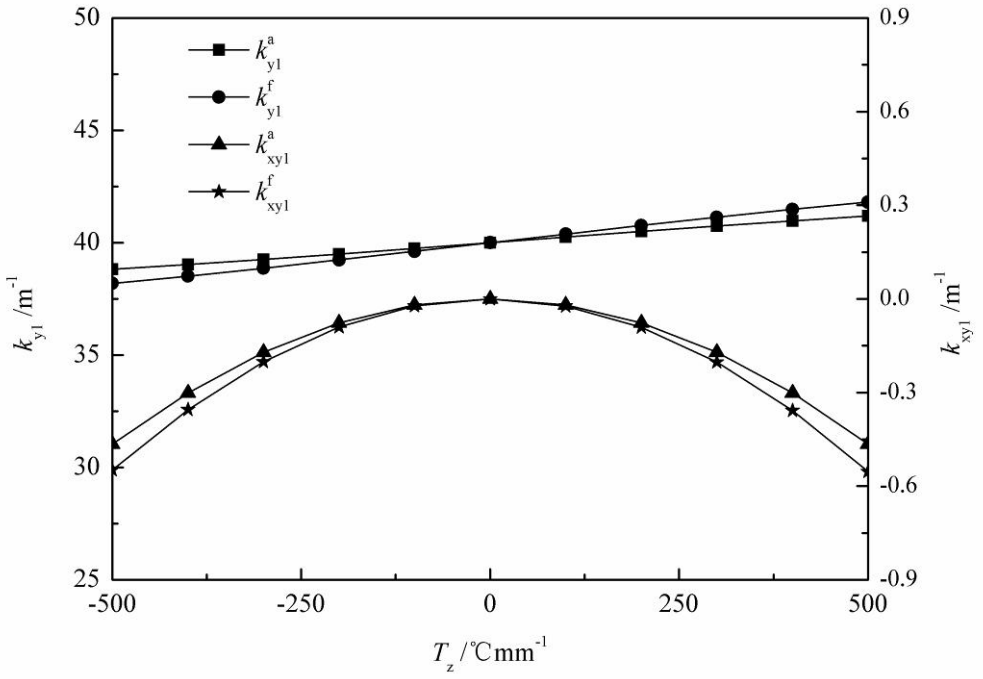

(a) Relationship of T_z and the curvatures of initial shape.

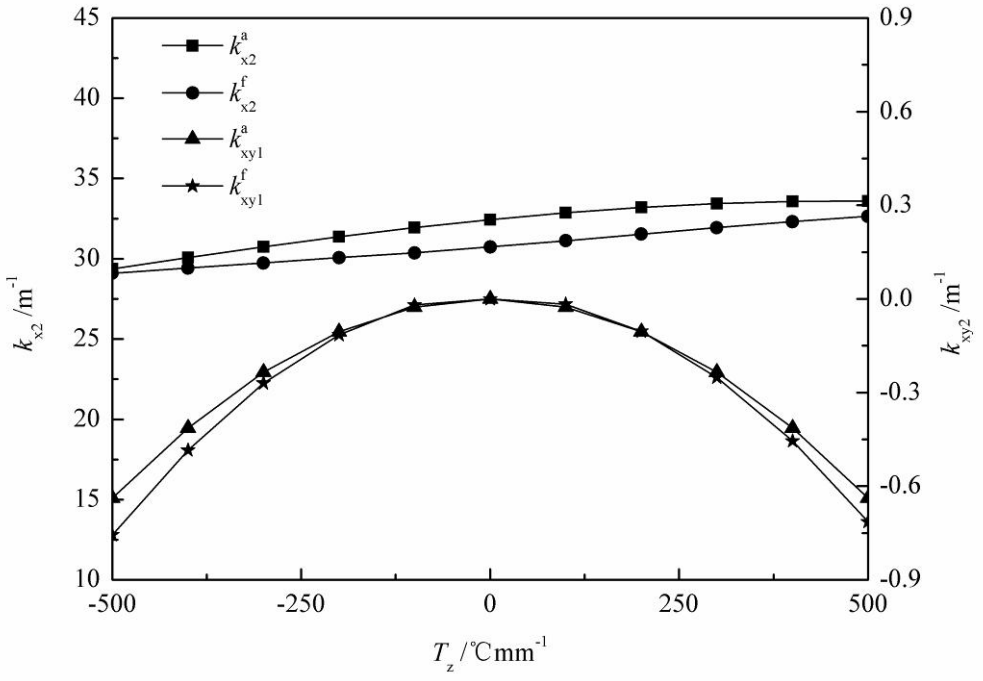

(b) Relationship of T_z and the curvatures of second stable shape.

Fig.9 Influence of T_z on the curvatures of the shell.

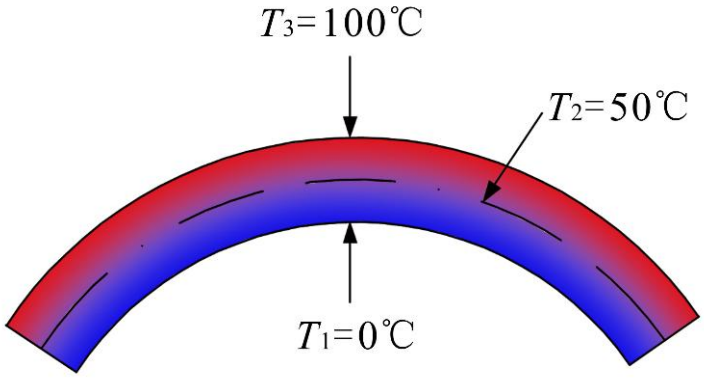

Fig. 10 Temperature distribution across shell's thickness (T_z = 200°Cmm^{-1}).

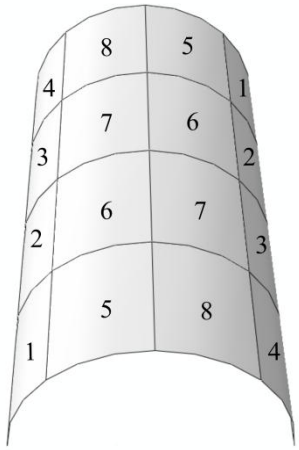

Fig.11 Partition of the shell model in FE simulation.

Table 1 Influence of temperature on the curvatures of the anti-symmetric shell

T/°C	k_{xy1}^{a} /m^{-1}	k_{xy1}^{f} /m^{-1}	k_{x2}^{a} /m^{-1}	k_{x2}^{f} /m^{-1}	k_{xy2}^{a} /m^{-1}	k_{xy2}^{f} /m^{-1}
20	0	0	27.01	24.28	0	0
40	0.47	0.46	27.94	25.4	0.8	0.99
60	0.93	0.90	28.84	26.46	1.59	1.69
80	1.37	1.31	29.71	27.47	2.34	2.24
100	1.78	1.70	30.55	28.43	3.06	2.68
120	2.16	2.06	31.34	29.34	3.72	3.03
150	2.64	2.50	32.44	30.61	4.58	3.42

where T is environmental temperature, superscript a and f represent the analytical and FE results, respectively.

Table 2 Complex impact of ΔT and T_z on the curvature of the anti-symmetric shell when T_z is applied in negative direction

ΔT / °C	T_z / °C mm^{-1}	k_{y1}^a /m^{-1}	k_{y1}^f /m^{-1}	k_{xy1}^a /m^{-1}	k_{xy1}^f /m^{-1}	k_{x2}^a /m^{-1}	k_{x2}^f /m^{-1}	k_{xy2}^a /m^{-1}	k_{xy2}^f /m^{-1}
30	200	40.55	40.94	0.62	0.62	29.20	26.99	1.08	1.22
30	-200	39.45	39.06	0.62	0.62	27.32	25.09	1.08	1.25
55	-300	39.22	38.64	1.07	1.06	27.83	26.07	1.88	1.85
80	-400	39.05	38.34	1.42	1.39	28.31	27.08	2.54	2.2
105	-500	38.97	38.19	1.65	1.61	28.79	28.1	3.01	2.35
105	500	41.03	41.78	1.65	1.63	32.42	31.66	3.01	2.31

Table 3 Influence of value and direction of T_z applied on all region of the shell when ΔT =130°C

Region	T_z /°C mm^{-1}	k_{y1} /m^{-1}	k_{xy1} /m^{-1}	k_{x2} /m^{-1}	k_{xy2} /m^{-1}
All	-800	37.90	1.14	28.59	1.59
	-600	38.25	1.71	29.06	2.35
	-400	38.74	2.14	29.52	2.94
	0	40.00	2.50	30.62	3.42
	400	41.22	2.15	31.98	2.91
	600	41.72	1.72	32.51	2.33
	800	42.13	1.16	32.71	1.59

Where the region of ‘All’ means that all the region of the shell is applied with T_z.

Table 4 Influence of temperature field imposed of T_z when ΔT =130°C

Region*	T_z /°C mm^{-1}	k_{y1} /m^{-1}	k_{xy1} /m^{-1}	k_{x2} /m^{-1}	k_{xy2} /m^{-1}
1		39.69	2.33	30.37	3.19
1,2		39.40	2.15	30.16	2.94
1,5		39.43	2.16	30.03	2.97
1,2,5,6	-800	38.86	1.82	29.52	2.47
3,4,7,8		38.89	1.82	29.54	2.56
1,2,3,5,6,7		38.33	1.47	29.01	2.01
All		37.90	1.14	28.59	1.59

* where the regions of 1~8 are given in Fig. 11.

Table 5 Influence of region with different directions of T_z when ΔT =130℃

Region	T_z /℃ mm^{-1}	k_{y1} /m^{-1}	k_{xy1} /m^{-1}	k_{x2} /m^{-1}	k_{xy2} /m^{-1}
1	-800	39.98	2.16	30.62	2.95
4	800				
1,2	-800	39.95	1.84	30.60	2.47
3,4	800				
1,2,5,6	-800	39.88	1.22	30.45	1.60
3,4,7,8	800				